

Manipulating Spectral Windings and Skin Modes through Nonconservative Couplings

Ningxin Kong,¹ Chenghe Yu,^{1,2} Yilun Xu,^{1,3} Matteo Fadel,⁴ Xinyao Huang,^{5,*} and Qiongyi He^{1,2,6,7}

¹*State Key Laboratory for Mesoscopic Physics, School of Physics,
Frontiers Science Center for Nano-optoelectronics,*

& Collaborative Innovation Center of Quantum Matter, Peking University, Beijing 100871, China

²*Hefei National Laboratory, Hefei 230088, China*

³*Beijing Academy of Quantum Information Sciences, Beijing 100193, China*

⁴*Department of Physics, ETH Zürich, 8093 Zürich, Switzerland*

⁵*School of Physics, Beihang University, Beijing 100191, China*

⁶*Collaborative Innovation Center of Extreme Optics,
Shanxi University, Taiyuan, Shanxi 030006, China*

⁷*Peking University Yangtze Delta Institute of Optoelectronics, Nantong 226010, Jiangsu, China*

The discovery of the non-Hermitian skin effect (NHSE) has revolutionized our understanding of wave propagation in non-Hermitian systems, highlighting unexpected localization effects beyond conventional theories. Here, we discover that NHSE, accompanied by multi-type spectral phases, can be induced by manipulating nonconservative couplings. By characterizing the spectrum through the windings of the energy bands, we demonstrate that band structures with identical, opposite, and even twisted windings can be achieved. These inequivalent types of spectra originate from the multi-channel interference resulting from the interplay between conservative and nonconservative couplings. Associated with the multi-type spectra, unipolar and bipolar NHSE with different eigenmode localizations can be observed. Additionally, our findings link the nonreciprocal transmission properties of the system to multiple spectral phases, indicating a connection with the skin modes. This work paves new pathways for investigating non-Hermitian topological effects and manipulating nonreciprocal energy flow.

Introduction.— Recent advancements in the study of non-Hermitian systems have garnered extensive interest due to their unique attributes and potential applications that extend beyond the realm of traditional Hermitian physics [1–5]. Non-Hermitian Hamiltonians, typically employed to describe systems that exchange energy with their environment, have revealed a number of intriguing phenomena [6–10]. Among these, the non-Hermitian skin effect (NHSE) results in localization of the eigenstates at the edges of the system, challenging conventional bulk-boundary correspondence and having profound theoretical and experimental implications [11–17]. In fact, characteristic signatures of the NHSE are directly reflected in the system’s spectrum, which displays complex band structures forming closed loops with nonzero windings in the quasi-energy space under periodic boundary conditions (PBC), distinctly different from those observed under open boundary conditions (OBC) [18, 19]. Experimentally, the NHSE has been demonstrated in various practical setups including optical systems [20, 21], acoustic systems [22, 23], and topoelectrical circuits [24, 25]. These studies have potential applications in directional amplifiers [26, 27], enhanced sensors [28, 29], and efficient energy harvesting [30], showcasing the real-world utility of this effect.

Recent studies extend the exploration of NHSE by delving into the phenomenon of bipolar NHSE, where eigenmode localization is observed on both sides of a system [31, 32]. Unlike traditional unipolar NHSE, characterized by the same band windings with one-sided eigenmode localization, bipolar NHSE exhibits multi-type

spectral phases associated with diverse eigenmode localization patterns [33]. It can manifest as separate loops with opposite windings in multi-band models [34, 35] or as twisted loops in single-band scenarios [36, 37], attracting growing research interest in exploring the rich spectral topology of non-Hermitian systems and enlightening the applications in nonreciprocal wave manipulations.

Traditionally, the realization of bipolar NHSE necessitates asymmetric coupling strengths that extend beyond nearest-neighbor couplings [38–40]. Here, we propose a different mechanism to realize and manipulate spectral windings and skin modes, namely through nonconservative couplings. Different from coherent couplings, nonconservative couplings connect elements of the systems indirectly through intermediates with gain or loss, exhibiting non-Hermitian characteristics in the phase terms of the couplings [41–45]. By considering a chain of resonance modes with conservative nearest-neighbor couplings and nonconservative next-nearest-neighbor couplings, we find that diverse spectra can appear by manipulating the nonconservative coupling phases. These include closed loops with the same and opposite windings, as well as twisted windings with two oppositely oriented loops, which arise by combining the nonconservative couplings with multi-channel interference provided by the chain. Associated with the multi-type spectra, unipolar and bipolar NHSE with different eigenmode localizations can be observed. To connect with the nonreciprocity performance, we also present evidence for a close link between the nonreciprocal transmission of the chain and multi-type spectral phases as well as NHSE.

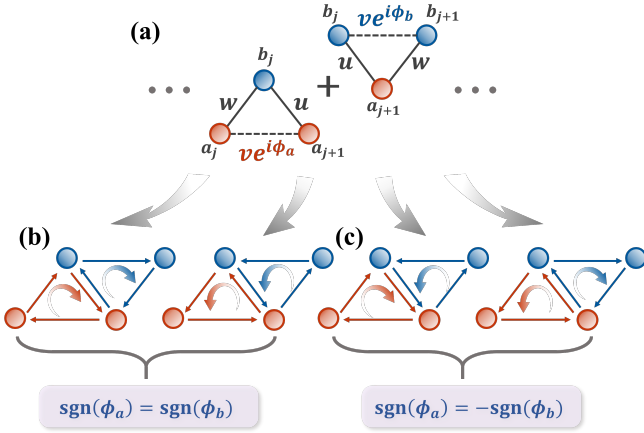


FIG. 1. (a) Schematic of the non-Hermitian chain with conservative nearest-neighbor couplings (solid lines) and non-conservative next-nearest-neighbor couplings ($ve^{i\phi_{a,b}}$, dashed lines). (b-c) Possible combinations of the upper and lower triangular plaquettes with the nonreciprocal flow. The direction of the nonreciprocal flow in each triangular plaquette (illustrated by the red and blue arrows) can be controlled by tuning the sign of the nonconservative coupling phases ϕ_a and ϕ_b .

Model.— We consider a chain of bosonic modes with conservative nearest-neighbor couplings and nonconservative next-nearest-neighbor couplings. The system Hamiltonian is given by

$$\begin{aligned} \hat{H} = & \sum_{j=1}^N [(\delta\hat{a}_j^\dagger\hat{a}_j - \delta\hat{b}_j^\dagger\hat{b}_j) + (w\hat{a}_j^\dagger\hat{b}_j + h.c.)] \\ & + \sum_{j=1}^{N-1} [(u\hat{b}_j^\dagger\hat{a}_{j+1} + h.c.) + ve^{i\phi_a}(\hat{a}_j^\dagger\hat{a}_{j+1} + h.c.)] \\ & + ve^{i\phi_b}(\hat{b}_j^\dagger\hat{b}_{j+1} + h.c.)], \end{aligned} \quad (1)$$

where 2δ is the difference of the mode resonance frequencies, w and u denote the conservative nearest-neighbor intra- and inter-hopping terms, respectively. The non-Hermiticity of the system is induced by considering nonzero phases ϕ_a and ϕ_b of the nonconservative next-nearest-neighbor couplings, where the energy flow in the coupling process $\hat{a}_j^\dagger\hat{a}_{j+1} + \hat{a}_{j+1}^\dagger\hat{a}_j$ ($\hat{b}_j^\dagger\hat{b}_{j+1} + \hat{b}_{j+1}^\dagger\hat{b}_j$) are not conserved (an example to implement the nonconservative couplings can be found in the Supplemental Material [46]). As illustrated in Fig. 1(a), this periodic coupling structure can be interpreted as a combination of the upper ($a_i \leftrightarrow b_i \leftrightarrow a_{i+1}$) and lower ($b_i \leftrightarrow a_{i+1} \leftrightarrow b_{i+1}$) triangular plaquettes. In each triangular plaquette, nonreciprocal energy flow can be realized by combining non-conservative couplings with two-channel interference provided by the nonzero effective flux [45]. The direction of the nonreciprocal flow in the triangular plaquette can be changed by tuning the sign of the nonconservative coupling phase ϕ_a (ϕ_b). When combining the upper and lower triangular plaquettes, the nonreciprocal

flow can be both clockwise (anti-clockwise) by choosing $\text{sgn}(\phi_a) = \text{sgn}(\phi_b)$, or in the opposite direction when $\text{sgn}(\phi_a) = -\text{sgn}(\phi_b)$, as shown in Fig. 1(b) and (c).

Multi-type spectra and NHSE.— Under the PBC, the Hamiltonian in Eq. (1) can be diagonalized in the momentum basis with $\hat{h}(k) = \langle k|\hat{H}|k\rangle = \sum_{a_j, b_j} \langle k, a_j|\hat{H}|k, b_j\rangle \langle a_j| \langle b_j|$, where $\hat{h}(k)$ denotes the momentum Hamiltonian. As shown in Fig. 2, the energy spectra under the PBC form loops in the complex quasi-energy space, which is distinct from the two open arcs under the OBC, indicating the emergence of the NHSE in our system [47]. To further investigate the energy spectra and wavefunctions of our model, we characterize the spectral phases by describing the band windings [18]. For any base point E_b , the winding number of the energy spectrum is given by

$$W = \frac{1}{2\pi i} \int_{-\pi}^{\pi} \partial_k \ln \det[\hat{h}(k) - E_b \cdot \mathbb{I}_{2 \times 2}] dk, \quad (2)$$

where $\mathbb{I}_{2 \times 2}$ is the two-dimensional identity matrix. The winding number is an integer obtained by counting the number of times that the eigenenergy of $\hat{h}(k)$ wraps around the base point E_b as k varies from $-\pi$ to π . When the loop structure is absent in the periodic spectrum, the energy base point E_b is not enclosed, resulting in $W = 0$ and the absence of the NHSE. The sign of the winding number is determined by the circling direction: anti-clockwise circling corresponds to $W = 1$ (left localization of eigenmodes), while clockwise circling corresponds to $W = -1$ (right localization of eigenmodes).

Characterizing the spectral topology by winding number W , we observe that the spectral phase diagrams of the two energy bands exhibit distinct behaviors when the nonconservative coupling phases ϕ_a and ϕ_b are adjusted, as depicted in Fig. 2 (a) and (b). The red and blue regions represent the closed-loop-like band structure with winding numbers $W = 1$ and $W = -1$ [Fig. 2(c) and (d)], respectively. The light yellow area indicates the presence of the twisted winding [Fig. 2(e) and (f)]. To elucidate the characteristics of spatial profiles corresponding to different spectral phases, we analyze the spatial profiles of all eigenmodes under the OBC, illustrated in Fig. 3. Based on the eigenmode distributions across the lattice sites in our model, these eigenmodes are categorized into two groups: those predominantly localized on sites a_j with minimal occupation on b_j , and vice versa. In the cases where $\text{sgn}(\phi_a) = \text{sgn}(\phi_b)$, the two bands typically exhibit opposite circling directions, as depicted in Fig. 2. Under these conditions, the eigenmodes predominantly occupying sites a_j localize toward the left edge, while the eigenmodes concentrated on sites b_j localize at the right boundary, simultaneously. This arrangement is indicative of the bipolar NHSE, as illustrated in Fig. 3 (a) and (b). Conversely, when $\text{sgn}(\phi_a) = -\text{sgn}(\phi_b)$, the two bands share the same winding number and circle in the same direction. This scenario results in all eigenmodes

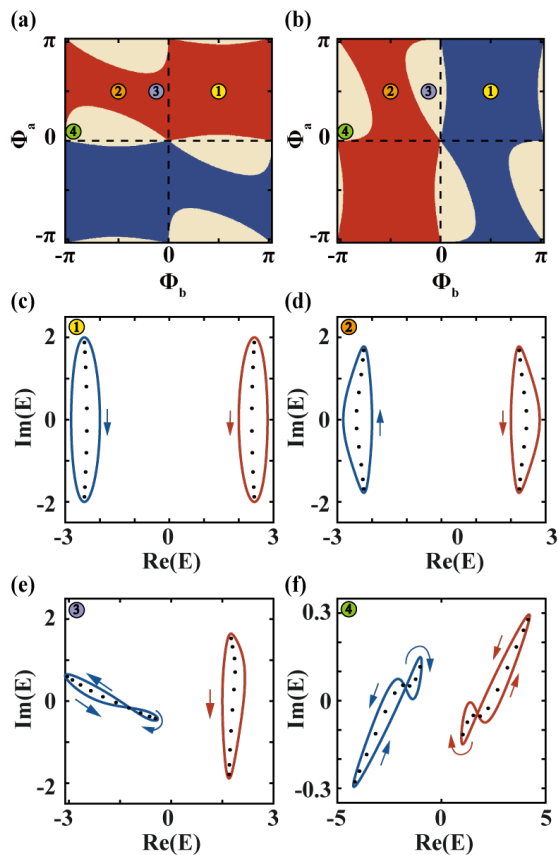


FIG. 2. (a)-(b) Phase diagram of the spectral winding number for the phase transition of two energy bands, respectively. The red region indicates the winding number $W = 1$ and the blue region indicates $W = -1$. The light yellow area represents the appearance of twisted spectral winding. (c)-(f) Spectra under PBC (red and blue for mode a and b) and OBC (black points) of the model, with different non-conservative coupling phases $\phi_b = \pi/2, -\pi/2, -\pi/8$ and $\phi_a = \pi/2$ (c)-(e), and $\phi_b = -19\pi/20, \pi/20, \phi_a = \pi/20$ (f), respectively. Clockwise and counterclockwise winding directions of the PBC spectrum versus the quasi-momentum k , as indicated by the arrows, correspond to OBC skin modes localized on the left and right, respectively. Other parameters are $\delta = 2, w = 1, u = i, v = 1$.

localizing at the same boundary, characteristic of the conventional unipolar NHSE, as shown in Fig. 3 (c) and (d).

Intriguingly, beyond the two regions mentioned above, there exists a unique spectrum type called twisted winding, which consists of two oppositely oriented loops in contact rather than a single loop. As illustrated in Fig. 2(e), the twisted loop splits the band into two segments, with one segment circling in a clockwise direction and the other in an anticlockwise direction, resulting in two opposite winding numbers within a single band. The corresponding distributions of all eigenmodes localized at both boundaries of the system are shown in Fig. 3(e). The other eigenmodes, corresponding to the spectrum with a single loop, are localized at the left boundary

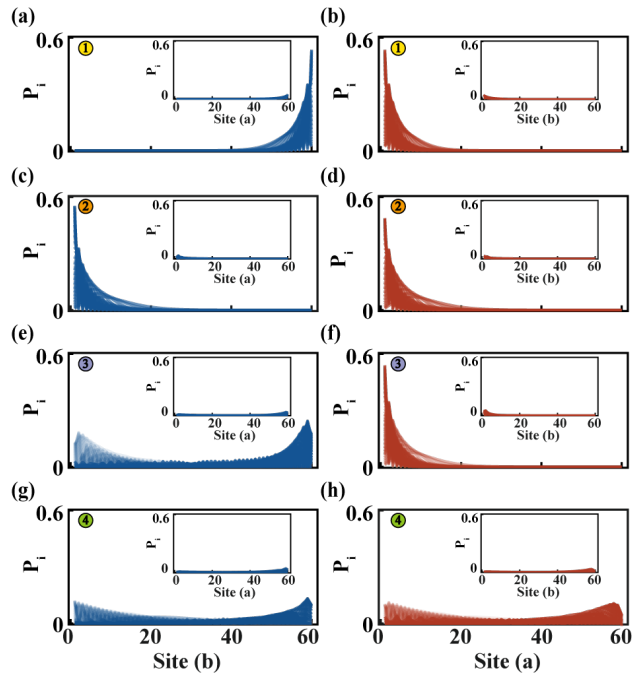


FIG. 3. (a)-(h) Distributions of all eigenmodes corresponding to the phase ①-④ in Fig. 2 respectively. Blue (red) lines represent the distributions of the eigenstates whose eigenvalue localized in the blue (red) loop of the PBC spectral on the b (a) sites. Insets show the distributions of eigenmodes on the a (b) sites, indicating a tiny population on the opposite side. Other parameters are $\delta = 2, w = 1, u = i, v = 1, N = 60$.

[Fig. 3(f)]. Simultaneous twisted loops in both bands can be induced by tuning the phases ϕ_a and ϕ_b , as shown in Fig. 2(f). In such cases, the eigenmodes associated with the twisted loops are split, localizing towards opposite boundaries, as depicted in Fig. 3(g)-(h). Moreover, the effects of the phase difference $(\phi_a - \phi_b)$ significantly influence the size of the twisting region in the phase space. Specifically, the region where $\text{sgn}(\phi_a) = -\text{sgn}(\phi_b)$ is considerably larger than that in which $\text{sgn}(\phi_a) = \text{sgn}(\phi_b)$.

The multi-type spectra and the NHSE localization transitions can also be observed in the context of the nonreciprocal flow in the periodic structure shown in Fig. 1. The band twisting is associated with the effective couplings between the upper and lower triangular plaquettes, specifically the energy flow between modes a_{j+1} and b_j . When the signs of ϕ_a and ϕ_b are the same, the opposite nonreciprocal flow from modes a_j to a_{j+1} and from b_{j+1} to b_j corresponds to the presence of the bipolar skin effects for $\text{sgn}(\phi_a) = \text{sgn}(\phi_b)$. In this scenario, the two nonreciprocal transmission channels between modes a_{j+1} and b_j , provided by the upper and lower triangular plaquettes, interfere destructively. This results in negligible energy flow between modes a_{j+1} and b_j , keeping the two bands relatively independent. Only when there is a significant difference between the phases ϕ_a and ϕ_b ,

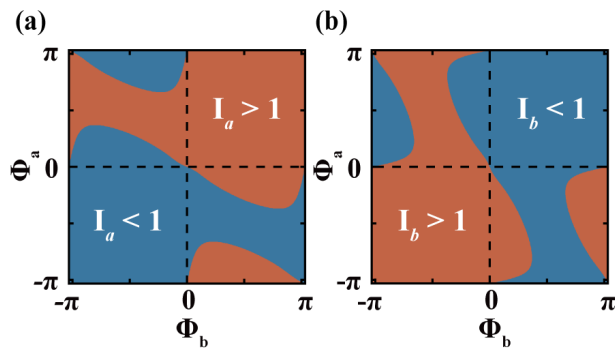


FIG. 4. Diagrams of nonreciprocity ratios as functions of the nonconservative coupling phases ϕ_a and ϕ_b , with the input/output field connected to mode a_1/a_N (a) and b_1/b_N (b). The red indicates the nonreciprocity ratio $I_{a/b} > 1$, and the blue region indicates $I_{a/b} < 1$. The size of the chain is $N = 4$ and the other parameters are the same as those presented in Fig. 2.

which results in a non-negligible effective coupling between the upper and lower triangular plaquettes, a band twist emerges. Conversely, when the signs of ϕ_a and ϕ_b differ, the nonreciprocal flows align, causing the same transmission from modes b_j to a_{j+1} in both the upper and lower triangular plaquettes. Constructive interference between these two transmission channels enhances the energy flow between the modes b_j and a_{j+1} , facilitating the twisting of the bands with even a small difference in the nonconservative coupling phases ϕ_a and ϕ_b .

Connection with nonreciprocity.— Extending the analysis of the connection between the nonreciprocity performance of the chain and the NHSE shown in different phase regions, we consider two different nonreciprocal transmission cases by choosing the leftmost mode a_1 (b_1) and rightmost mode a_N (b_N) to connect the input and output field, respectively. Therefore, the nonreciprocity ratios of the two cases can be defined as $I_a = T_{a\leftarrow}/T_{a\rightarrow} = |S_{1,2N-1}/S_{2N-1,1}|^2$, $I_b = T_{b\leftarrow}/T_{b\rightarrow} = |S_{2,2N}/S_{2N,2}|^2$, which can be calculated by solving the system scattering matrix S numerically (see the Supplemental Material for more details [46]). Once the off-diagonal elements of S satisfy $|S_{1,2N-1}| \neq |S_{2N-1,1}|$ ($|S_{2,2N}| \neq |S_{2N,2}|$), the nonreciprocal transmission in the chain can be achieved. When the transmission efficiency for the backward (forward) direction is larger than that for the forward (backward) direction for the chain, i.e., $I_{a/b} > 1$ ($I_{a/b} < 1$), the nonreciprocity direction of the chain is on the backward (forward). The nonreciprocity ratios of the two different settings that the input/output field connecting with the mode a_1/a_N and b_1/b_N are illustrated in Fig. 4 (a) and (b), respectively. The red (blue) region represents the nonreciprocity ratio $I_{a/b} > 1$ ($I_{a/b} < 1$), indicating the backward (forward) nonreciprocity direction for the chain. Comparing the spectral phase diagram shown in Fig. 2 (a) and (b), we can find the nonrecipro-

cal transmission shows similar behaviors with the eigenmode localization of NHSE. When tuning the phases as $\text{sgn}(\phi_a) = -\text{sgn}(\phi_b) < 0$ and $|\phi_a|$ and $|\phi_b|$ are around $\pi/2$, both I_a and I_b are greater than 1 for left eigenmode localization and less than 1 for right eigenmode localization of unipolar NHSE. However, the nonreciprocity directions of the two input/output settings will become opposite when tuning the nonconservative coupling phases to the region of closed loops with opposite windings. We can find that the nonreciprocity ratio $I_a > 1$ while $I_b < 1$ when $\text{sgn}(\phi_a) = \text{sgn}(\phi_b) > 0$, and $I_a < 1$ while $I_b > 1$ when $\text{sgn}(\phi_a) = \text{sgn}(\phi_b) < 0$ [Fig. 4 (a) and (b)]. Therefore, the opposite nonreciprocity directions of the two settings can connect with the opposite localization of the two groups of eigenmodes, indicating a close link between the bipolar NHSE and nonreciprocity. In addition, when approaching the band twisting region, the change of the nonreciprocity direction is determined by the values of the nonconservative coupling phases and the chain size N together (see the Supplemental Material for more details [46]).

Conclusion.— In conclusion, we elucidated the manipulation of the NHSE through nonconservative couplings that extend beyond nearest-neighbor couplings, demonstrating multi-type spectral phases and their impact on mode localizations. By tuning the phases of the nonconservative couplings, we achieved diverse spectral structures associated with both unipolar and bipolar NHSE localizations. Moreover, we have evidenced that multi-type spectral phases as well as NHSE are closely linked to the nonreciprocal transmission of the chain. Our approach is also experimentally feasible as nonconservative couplings have been realized in various systems, including optical systems [48, 49], room-temperature atomic ensembles [50] and magnonics system [51, 52]. Our findings not only provide new insights into the control of NHSE but also pave the way for advanced applications in controlling nonreciprocal energy flow.

Acknowledgement.— This work is supported by the Beijing Natural Science Foundation (Grant No. Z240007), National Natural Science Foundation of China (Grants No. 12104252, No. 12125402), and the Innovation Program for Quantum Science and Technology (Grant No. 2021ZD0301500).

* xinyahuang@buaa.edu.cn

- [1] C. M. Bender, Making sense of non-hermitian hamiltonians, *Rep. Prog. Phys.* **70**, 947 (2007).
- [2] Z. Gong, Y. Ashida, K. Kawabata, K. Takasan, S. Higashikawa, and M. Ueda, Topological phases of non-hermitian systems, *Phys. Rev. X* **8**, 031079 (2018).
- [3] Z. G. Yuto Ashida and M. Ueda, Non-hermitian physics, *Adv. Phys.* **69**, 249 (2020).
- [4] E. J. Bergholtz, J. C. Budich, and F. K. Kunst, Ex-

- ceptional topology of non-hermitian systems, *Rev. Mod. Phys.* **93**, 015005 (2021).
- [5] N. Okuma and M. Sato, Non-hermitian topological phenomena: A review, *Annu. Rev. Condens. Matter Phys.* **14**, 83 (2023).
- [6] Z.-P. Liu, J. Zhang, i. m. c. K. Özdemir, B. Peng, H. Jing, X.-Y. Lü, C.-W. Li, L. Yang, F. Nori, and Y.-x. Liu, Metrology with \mathcal{PT} -symmetric cavities: Enhanced sensitivity near the \mathcal{PT} -phase transition, *Phys. Rev. Lett.* **117**, 110802 (2016).
- [7] H. Xu, D. Mason, L. Jiang, and J. G. E. Harris, Topological energy transfer in an optomechanical system with exceptional points, *Nature* **537**, 80 (2016).
- [8] R. El-Ganainy, K. G. Makris, M. Khajavikhan, Z. H. Musslimani, S. Rotter, and D. N. Christodoulides, Non-hermitian physics and PT symmetry, *Nat. Phys.* **14**, 11 (2018).
- [9] Ş. K. Özdemir, S. Rotter, F. Nori, and L. Yang, Parity-time symmetry and exceptional points in photonics, *Nat. Mater.* **18**, 783 (2019).
- [10] A. Li, H. Wei, M. Cotrufo, W. Chen, S. Mann, X. Ni, B. Xu, J. Chen, J. Wang, S. Fan, C.-W. Qiu, A. Alù, and L. Chen, Exceptional points and non-hermitian photonics at the nanoscale, *Nat. Nanotechnol.* **18**, 706 (2023).
- [11] S. Yao and Z. Wang, Edge states and topological invariants of non-hermitian systems, *Phys. Rev. Lett.* **121**, 086803 (2018).
- [12] Q. Liang, D. Xie, Z. Dong, H. Li, H. Li, B. Gadway, W. Yi, and B. Yan, Dynamic signatures of non-hermitian skin effect and topology in ultracold atoms, *Phys. Rev. Lett.* **129**, 070401 (2022).
- [13] M.-H. L. Xiujuan Zhang, Tian Zhang and Y.-F. Chen, A review on non-hermitian skin effect, *Adv. Phys.: X* **7**, 2109431 (2022).
- [14] Z. Yang, K. Zhang, C. Fang, and J. Hu, Non-hermitian bulk-boundary correspondence and auxiliary generalized brillouin zone theory, *Phys. Rev. Lett.* **125**, 226402 (2020).
- [15] W. Wang, X. Wang, and G. Ma, Non-hermitian morphing of topological modes, *Nature* **608**, 50 (2022).
- [16] L. Li, C. H. Lee, S. Mu, and J. Gong, Critical non-hermitian skin effect, *Nat. Commun.* **11**, 5491 (2020).
- [17] R. Lin, T. Tai, L. Li, and C. H. Lee, Topological non-hermitian skin effect, *Front. Phys.* **18**, 53605 (2023).
- [18] K. Zhang, Z. Yang, and C. Fang, Correspondence between winding numbers and skin modes in non-hermitian systems, *Phys. Rev. Lett.* **125**, 126402 (2020).
- [19] K. Ding, C. Fang, and G. Ma, Non-hermitian topology and exceptional-point geometries, *Nat. Rev. Phys.* **4**, 745 (2022).
- [20] Y. Li, C. Liang, C. Wang, C. Lu, and Y.-C. Liu, Gain-loss-induced hybrid skin-topological effect, *Phys. Rev. Lett.* **128**, 223903 (2022).
- [21] L. Xiao, T. Deng, K. Wang, G. Zhu, Z. Wang, W. Yi, and P. Xue, Non-hermitian bulk-boundary correspondence in quantum dynamics, *Nat. Phys.* **16**, 761 (2020).
- [22] L. Zhang, Y. Yang, Y. Ge, Y.-J. Guan, Q. Chen, Q. Yan, F. Chen, R. Xi, Y. Li, D. Jia, S.-Q. Yuan, H.-X. Sun, H. Chen, and B. Zhang, Acoustic non-hermitian skin effect from twisted winding topology, *Nat. Commun.* **12**, 6297 (2021).
- [23] X. Zhang, Y. Tian, J.-H. Jiang, M.-H. Lu, and Y.-F. Chen, Observation of higher-order non-hermitian skin effect, *Nat. Commun.* **12**, 5377 (2021).
- [24] T. Helbig, T. Hofmann, S. Imhof, M. Abdelghany, T. Kiessling, L. W. Molenkamp, C. H. Lee, A. Szameit, M. Greiter, and R. Thomale, Generalized bulk-boundary correspondence in non-hermitian topoelectrical circuits, *Nat. Phys.* **16**, 747 (2020).
- [25] D. Zou, T. Chen, W. He, J. Bao, C. H. Lee, H. Sun, and X. Zhang, Observation of hybrid higher-order skin-topological effect in non-hermitian topoelectrical circuits, *Nat. Commun.* **12**, 7201 (2021).
- [26] P. Wen, M. Wang, and G.-L. Long, Optomechanically induced transparency and directional amplification in a non-hermitian optomechanical lattice, *Opt. Express* **30**, 41012 (2022).
- [27] M. Tian, F. Sun, K. Shi, H. Xu, Q. He, and W. Zhang, Nonreciprocal amplification transition in a topological photonic network, *Photon. Res.* **11**, 852 (2023).
- [28] A. McDonald and A. A. Clerk, Exponentially-enhanced quantum sensing with non-hermitian lattice dynamics, *Nat. Commun.* **11**, 5382 (2020).
- [29] J. C. Budich and E. J. Bergholtz, Non-hermitian topological sensors, *Phys. Rev. Lett.* **125**, 180403 (2020).
- [30] W.-T. Xue, Y.-M. Hu, F. Song, and Z. Wang, Non-hermitian edge burst, *Phys. Rev. Lett.* **128**, 120401 (2022).
- [31] F. Song, S. Yao, and Z. Wang, Non-hermitian topological invariants in real space, *Phys. Rev. Lett.* **123**, 246801 (2019).
- [32] H. Xin, W. Song, S. Wu, Z. Lin, S. Zhu, and T. Li, Manipulating the non-hermitian skin effect in optical ring resonators, *Phys. Rev. B* **107**, 165401 (2023).
- [33] T. Zhang, X. Zhang, M.-H. Lu, and Y.-F. Chen, Multiple phase transitions and anomalous non-hermitian skin effect, *Phys. Rev. B* **107**, 094111 (2023).
- [34] Z. Lin, W. Song, L.-W. Wang, H. Xin, J. Sun, S. Wu, C. Huang, S. Zhu, J.-H. Jiang, and T. Li, Observation of topology transition in floquet non-hermitian skin effects in silicon photonics, *arXiv:2402.09700* (2024).
- [35] D. Liu, Z. Wang, Z. Cheng, H. Hu, Q. Wang, H. Xue, B. Zhang, and Y. Luo, Simultaneous manipulation of line-gap and point-gap topologies in non-hermitian lattices, *Laser Photonics Rev.* **17**, 2200371 (2023).
- [36] C. Yuce and H. Ramezani, Strong edge burst with bipolar non-hermitian skin effect, *Phys. Rev. B* **109**, 214301 (2024).
- [37] W. Li, Z. Sun, Z. Yang, and F. Li, Universal scalefree non-hermitian skin effect near the bloch point, *Phys. Rev. B* **109**, 035119 (2024).
- [38] K. Wang, A. Dutt, K. Y. Yang, C. C. Wojcik, J. Vučković, and S. Fan, Generating arbitrary topological windings of a non-hermitian band, *Science* **371**, 1240 (2021).
- [39] K. Wang, A. Dutt, C. C. Wojcik, and S. Fan, Topological complex-energy braiding of non-hermitian bands, *Nature* **598**, 59 (2021).
- [40] S. M. Rafi-Ul-Islam, Z. B. Siu, H. Sahin, M. S. H. Razo, and M. B. A. Jalil, Twisted topology of non-hermitian systems induced by long-range coupling, *Phys. Rev. B* **109**, 045410 (2024).
- [41] F. Yang, Y.-C. Liu, and L. You, Anti- \mathcal{PT} symmetry in dissipatively coupled optical systems, *Phys. Rev. A* **96**, 053845 (2017).
- [42] C. Leefmans, A. Dutt, J. Williams, L. Yuan, M. Parto, F. Nori, S. Fan, and A. Marandi, Topological dissipation

- in a time-multiplexed photonic resonator network, *Nat. Phys.* **18**, 442 (2022).
- [43] A. Metelmann and A. A. Clerk, Nonreciprocal photon transmission and amplification via reservoir engineering, *Phys. Rev. X* **5**, 021025 (2015).
- [44] X. Huang, C. Lu, C. Liang, H. Tao, and Y.-C. Liu, Loss-induced nonreciprocity, *Light: Sci. Appl.* **10**, 30 (2021).
- [45] X. Huang and Y.-C. Liu, Perfect nonreciprocity by loss engineering, *Phys. Rev. A* **107**, 023703 (2023).
- [46] Supplemental material., See Supplemental Material at XXX for details on the derivation of the effective Hamiltonian with nonconservative couplings, the nonreciprocal energy transmission, the phase diagram of two-band winding number and Inverse Participation Ratio (IPR) and the influence of the nonconservative coupling strength on the twisting region.
- [47] N. Okuma, K. Kawabata, K. Shiozaki, and M. Sato, Topological origin of non-hermitian skin effects, *Phys. Rev. Lett.* **124**, 086801 (2020).
- [48] G. Arwas, S. Gadasi, I. Gershenzon, A. Friesem, N. Davidson, and O. Raz, Anyonic-parity-time symmetry in complex-coupled lasers, *Sci. Adv.* **8**, eabm7454 (2022).
- [49] A. Bergman, R. Duggan, K. Sharma, M. Tur, A. Zadok, and A. Alù, Observation of anti-parity-time-symmetry, phase transitions and exceptional points in an optical fibre, *Nat. Commun.* **12**, 486 (2021).
- [50] P. Peng, W. Cao, C. Shen, W. Qu, J. Wen, L. Jiang, and Y. Xiao, Anti-parity-time symmetry with flying atoms, *Nat. Phys.* **12**, 1139 (2016).
- [51] Y. Yang, Y.-P. Wang, J. W. Rao, Y. S. Gui, B. M. Yao, W. Lu, and C.-M. Hu, Unconventional singularity in anti-parity-time symmetric cavity magnonics, *Phys. Rev. Lett.* **125**, 147202 (2020).
- [52] J. Zou, S. Bosco, E. Thingstad, J. Klinovaja, and D. Loss, Dissipative spin-wave diode and nonreciprocal magnonic amplifier, *Phys. Rev. Lett.* **132**, 036701 (2024).